COMMUNICATIONS IN COMPUTATIONAL PHYSICS
Vol. **2**, No. 2, pp. 334-357

Commun. Comput. Phys.
April 2007

# An Efficient Real Space Method for Orbital-Free Density-Functional Theory

Carlos J. García-Cervera*

*Department of Mathematics, University of California, Santa Barbara, CA 93106, USA.*

Received 3 July 2006; Accepted (in revised version) 9 August 2006

Communicated by Weinan E

Available online 30 September 2006

**Abstract.** We consider the Thomas-Fermi-von Weizsacker energy functional, with the Wang-Teter correction, and present an efficient real space method for Orbital-Free Density Functional Theory. It is proved that the energy minimizer satisfies a second order quasilinear elliptic equation, even at the points where the electron density vanishes. This information is used to construct an efficient energy minimization method for the resulting constrained problem, based on the truncated Newton method for unconstrained optimization. The Wang-Teter kernel is analyzed, and its behavior in real space at short and far distances is determined. A second order accurate discretization of the energy is obtained using finite differences. The efficiency and accuracy of the method is illustrated with numerical simulations in an Aluminium FCC lattice.

**Key words**: Density functional theory; truncated Newton method; constrained optimization.

## 1 Introduction

All material properties in a solid derive from the interactions between its constituent atoms. A full description of such interactions requires the solution of Schrödinger's equation in an ambient space of dimension $3N$, where $N$ is the number of particles. In the Born-Oppenheimer approximation the positions of the nuclei of the atoms are fixed, so $N$ represents the total number of electrons.

It was first realized by Thomas [1] and Fermi [2] that the electronic structure of solids in their ground state could be fully understood in terms of the electron density alone, $\rho$.

*Correspondence to: Carlos J. García-Cervera, Department of Mathematics, University of California, Santa Barbara, CA 93106, USA. Email:cgarcia@math.ucsb.edu

 

This fact, which gave origin to Density-Functional Theory (DFT), was later formalized by Hohenberg and Kohn [3, 4]. In [3] it was proved that there exists a functional of the density $F[\rho]$, such that the ground state energy associated to an external potential $v$ can be obtained by minimizing the energy

$$E[\rho] = F[\rho] + \int_\Omega v(\mathbf{x})\rho(\mathbf{x})\, d\mathbf{x}, \tag{1.1}$$

where $\Omega$ may be a bounded domain, a periodic cell, or the whole space. The exact form of $F[\rho]$, however, is not known. Kohn and Sham [5] presented an approximation scheme for $F[\rho]$, and wrote the energy as

$$E[\rho] = F_s[\rho] + F_H[\rho] + F_{XC}[\rho] + \int_\Omega v(\mathbf{x})\rho(\mathbf{x})\, d\mathbf{x}, \tag{1.2}$$

where $F_s[\rho]$ is the exact kinetic energy of a system of non-interacting electrons with density $\rho$. The other contributions to the energy in (1.2) are Hartree, exchange and correlation, and external potential energies, respectively.

The Hartree energy describes the Coulombic interactions between electrons:

$$F_H[\rho] = \frac{1}{2}\int_\Omega\int_\Omega \frac{\rho(\mathbf{x})\rho(\mathbf{y})}{|\mathbf{x}-\mathbf{y}|}\, d\mathbf{x}\, d\mathbf{y} = \frac{1}{2}\int_\Omega \rho\, K_H * \rho, \tag{1.3}$$

where we have defined $K_H(\mathbf{x}) = |\mathbf{x}|^{-1}$.

The exchange and correlation energy, $F_{XC}[\rho]$, introduces corrections to the energy that derive from using the non-interacting electron approximation for the kinetic and Hartree energies. Although the expression for the total energy in (1.2) is exact, $F_{XC}[\rho]$ is unknown. Here we approximate $F_{XC}[\rho]$ using the local density approximation (LDA) [4, 5]:

$$F_{XC}[\rho] = \int_\Omega f(\rho), \tag{1.4}$$

where $f(\rho)$ is given in (2.1) below.

The last term in energy (1.2) represents the effect of an external potential. In what follows we consider $\rho$ to be the density of the valence electrons only. The core electrons and the nuclei are treated as a unit which interacts with the valence electrons through the pseudopotential $v(\mathbf{x})$.

The exact computation of the Kohn-Sham kinetic energy functional requires the computation of the $N$ non-interacting electron orbitals, which is equivalent to solving a system of $N$ coupled Schrödinger equations in $\mathbb{R}^3$. In the spirit of the Thomas-Fermi approach, it is desirable to approximate the kinetic energy by a functional of the density alone, free of orbitals. Several such approximations have been proposed in what is called Orbital-Free Density-Functional Theory (OFDFT) [1,2,6–10]. We consider the Thomas-Fermi-von Weizsacker kinetic energy functional, with the additional correction of Wang and Teter [7]:

$$F_s[\rho] = \frac{1}{8}\int_\Omega \frac{|\nabla\rho|^2}{\rho} + C_{TF}\int_\Omega \rho^{5/3} + F_{WT}[\rho]. \tag{1.5}$$

In (1.5), the Thomas-Fermi constant has the value $C_{TF} = \frac{3}{10}(2\pi^2)^{1/3}$. The Wang-Teter kinetic energy is

$$F_{WT}[\rho] = -\frac{32C_{TF}}{25}\int_\Omega \rho^{5/3} + \frac{4C_{TF}}{5}\int_\Omega \rho^{5/6} K_{WT} * \rho^{5/6}. \tag{1.6}$$

The convolution kernel, $K_{WT}$, is given in Fourier space in terms of the Lindhard susceptibility function,

$$\widehat{K_{WT}}(\eta) = \left(\frac{1}{2} + \frac{1-\eta^2}{4\eta}\ln\left|\frac{1+\eta}{1-\eta}\right|\right)^{-1} - 3\eta^2 + \frac{3}{5}, \tag{1.7}$$

where $\eta = |\xi|/(2k_F)$, $k_F = (3\pi^2\rho_0)^{1/3}$ is the Fermi wave vector, and $\rho_0$ is the average electron density [7]. A generalization of (1.6) to density-dependent kernels has been presented recently by Wang, Govind, and Carter [8].

In this article we consider $\Omega$ to be a finite domain containing the solid, and set the density to be zero on the boundary. Energy functional (1.2) must be minimized in the admissible class

$$\mathcal{A} = \left\{\rho \geq 0,\ \int_\Omega \rho = N,\ \rho^{-1/2}\nabla\rho \in L_2(\Omega)\right\}, \tag{1.8}$$

where $L_2(\Omega)$ represents the set of square integrable functions.

The presence of $\rho$ in the denominator in the kinetic energy (1.5) can result in numerical instabilities. A more regular expression for the energy can be obtaining noting that

$$\frac{1}{8}\frac{|\nabla\rho|^2}{\rho} = \frac{1}{2}|\nabla\sqrt{\rho}|^2. \tag{1.9}$$

This suggests the change $u = \sqrt{\rho}/\sqrt{N}$; rescaling the energy by the number of electrons we obtain the energy per electron

$$\begin{aligned} F[u] &= \frac{1}{N}E[Nu^2] = \frac{1}{2}\int_\Omega |\nabla u|^2 - \frac{7C_{TF}N^{2/3}}{25}\int_\Omega u^{10/3} \\ &+\frac{4C_{TF}N^{2/3}}{5}\int_\Omega |u|^{5/3} K_{WT} * |u|^{5/3} + \frac{N}{2}\int_\Omega u^2\, K_H * u^2 \\ &-\frac{3}{4}\left(\frac{3N}{\pi}\right)^{1/3}\int_\Omega u^{8/3} + \int_\Omega u^2\varepsilon(Nu^2) + \int_\Omega v(\mathbf{x})u^2(\mathbf{x})\,d\mathbf{x}. \end{aligned} \tag{1.10}$$

Functional (1.10) must be minimized among functions in

$$\mathcal{B} = \left\{u \in H_0^1(\Omega)\middle| u \geq 0,\ \int_\Omega u^2 = 1\right\}, \tag{1.11}$$

where

$$H_0^1(\Omega) = \{u \in L_2(\Omega) | \frac{\partial u}{\partial x_i} \in L_2(\Omega), i = 1, \ldots, n, \text{ and } u = 0 \text{ on } \partial\Omega\}.$$

The remainder of this article is organized as follows: In Section 2 we describe the exchange and correlation, pseudopotential, Hartree, and Wang-Teter terms in more detail. We prove that minimizers exist, and in addition we prove that the minimizers satisfy an elliptic equation, even at the points where the density vanishes. In Section 3 we present a modification of the Truncated-Newton method for energy minimization applied to the constrained problem (1.10)-(1.11). The efficiency and accuracy of the method is illustrated with several examples in Section 4.

## 2 Existence of minimizers and basic properties

### 2.1 Exchange and correlation energy

In the LDA, the exchange and correlation energy is approximated using an expression that depends only on the value of the density of the form

$$F_{XC}[\rho] = -\frac{3}{4}\left(\frac{3}{\pi}\right)^{1/3}\int \rho^{4/3} + \int \rho\varepsilon(\rho). \tag{2.1}$$

The first term in (2.1) is an expression for the quantum mechanical exchange energy [4]. For the second term we use the expression derived by Perdew and Zunger [11]:

$$\varepsilon(r_s) = \begin{cases} \dfrac{\gamma}{1+\beta_1\sqrt{r_s}+\beta_2 r_s}, & r_s \geq 1, \\ A\ln(r_s) + B + Cr_s\ln(r_s) + Dr_s, & r_s \leq 1. \end{cases} \tag{2.2}$$

In (2.2), $r_s = (\frac{3}{4\pi\rho})^{1/3}$; the parameters used are $\gamma = -0.1423$, $\beta_1 = 1.0529$, $\beta_2 = 0.3334$, $A = 0.0311$, $B = -0.048$, and $C = 2.019151940622 \times 10^{-3}$ and $D = -1.163206637891 \times 10^{-2}$ are chosen so that $\varepsilon(r)$ and $\varepsilon'(r)$ are continuous at $r = 1$ [11]. The function $\varepsilon$ and its derivative are plotted in Fig. 1. We plot the energy density $\rho\varepsilon$ and its derivative in Fig. 2. Note that $\rho\varepsilon \to 0$ as $\rho \to 0$, and $\rho\varepsilon \sim -\frac{A}{3}\rho\log(\rho) + \mathcal{O}(\rho)$ as $\rho \to \infty$.

### 2.2 Wang-Teter convolution kernel

The Wang-Teter convolution kernel is given in terms of the Lindhard susceptibility function [7, 8]:

$$\widehat{K_{WT}}(\eta) = \frac{1}{\frac{1}{2} + \frac{1-\eta^2}{4\eta}\log\left|\frac{1+\eta}{1-\eta}\right|} - 3\eta^2 + \frac{3}{5}. \tag{2.3}$$

Function (2.3) is plotted in Fig. 3. As $\eta \to \infty$,

$$\widehat{K_{WT}}(\eta) = -\frac{24}{175}\frac{1}{\eta^2} - \frac{8}{125}\frac{1}{\eta^4} - \frac{37}{625}\frac{1}{\eta^6} + \mathcal{O}\left(\frac{1}{\eta^8}\right). \tag{2.4}$$

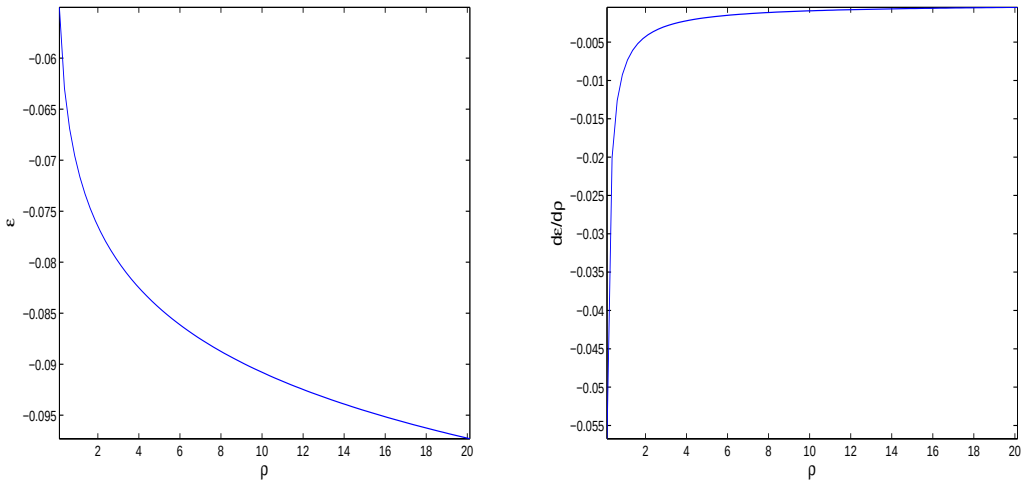


(a) (b)

Figure 1: Perdew and Zunger's parameterization of the correlation function [11]. (a) Function $\varepsilon$, and (b) its derivative, $d\varepsilon/d\rho$.

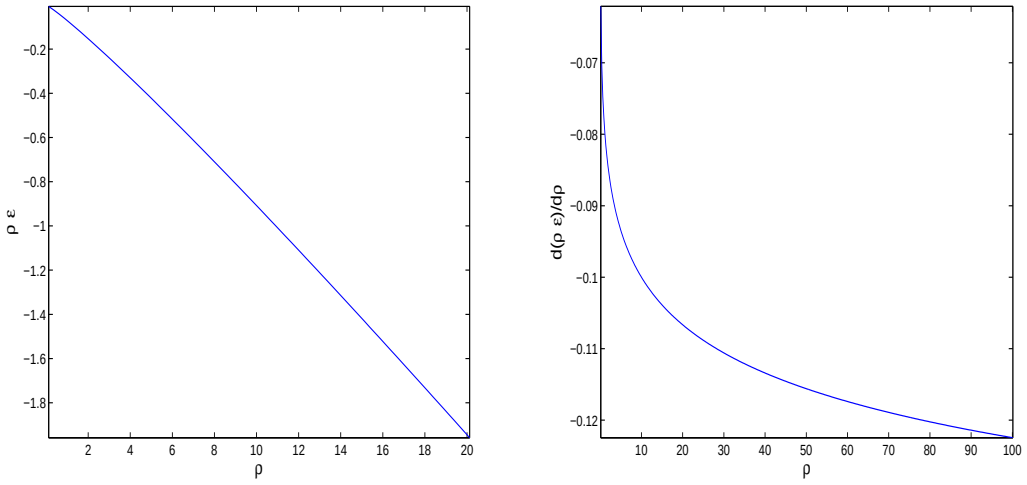


(a) (b)

Figure 2: Perdew and Zunger's parameterization of the correlation energy density [11]. (a) Energy density $\rho\varepsilon$, and (b) its derivative, $d(\rho\varepsilon)/d\rho$.

Since the Fourier transform of the kernel only decays quadratically, it follows that the Wang-Teter kernel is singular at $\mathbf{x} = 0$. In order to understand the behavior of the kernel near zero, we decompose the kernel into two parts:

$$K_{WT} = K_{WT}^{I} + K_{WT}^{II}. \tag{2.5}$$

The first contribution, $K_{WT}^{I}$, is singular at $\mathbf{x} = 0$, whereas $K_{WT}^{II}$ is bounded. In Fourier

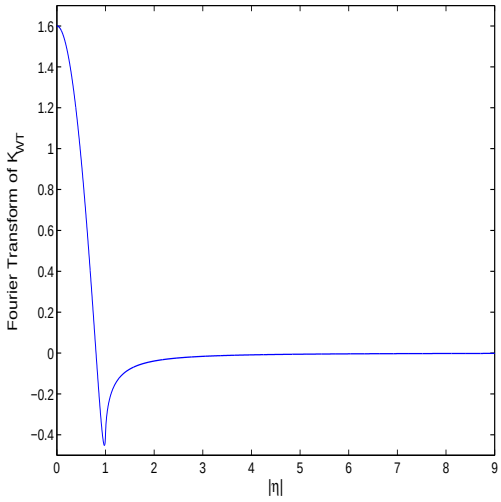


Figure 3: Fourier Transform of the Wang-Teter kernel. The kernel is not differentiable at $\eta = 1$, and decays like $|\eta|^{-2}$.

space, $K^I_{WT}$ is a rational function of the form

$$\widehat{K^I_{WT}}(\eta) = \frac{A\eta^2}{\eta^4 + B\eta^2 + C}, \tag{2.6}$$

where the constants $A$, $B$, and $C$ are chosen to capture the decay of the Wang-Teter kernel:

$$\widehat{K^I_{WT}}(\eta) = -\frac{24}{175}\frac{1}{\eta^2} - \frac{8}{125}\frac{1}{\eta^4} + \mathcal{O}\left(\frac{1}{\eta^6}\right), \quad \text{as } |\eta| \to \infty. \tag{2.7}$$

If we insist on capturing also the $\mathcal{O}(\eta^{-6})$ term, the rational function has a pole on the real axis. Therefore, we only consider the $\mathcal{O}(\eta^{-2})$ and $\mathcal{O}(\eta^{-4})$ terms, which leaves $C$ undetermined. To prevent the existence of poles on the real axis, and to simplify the Fourier inversion of $\widehat{K^I_{WT}}$, we arbitrarily choose $C = B^2$. The parameters are therefore

$$A = -\frac{24}{175}; \quad B = -\frac{7}{15}; \quad C = B^2. \tag{2.8}$$

Since $\widehat{K^I_{WT}}$ only depends on $|\eta|$, $K^I_{WT}$ is also radially symmetric. Therefore

$$\begin{aligned} K^I_{WT}(|\mathbf{x}|) &= \frac{1}{(2\pi)^3}\int_{\mathbb{R}} e^{i\xi_3|\mathbf{x}|}\widehat{K^I_{WT}}(|\eta|)\,d\eta \\ &= \frac{1}{4\pi^2}\int_{-\frac{\pi}{2}}^{\frac{\pi}{2}}\int_0^\infty e^{ir\sin(\theta)|\mathbf{x}|}\frac{Ar^4\cos(\theta)}{r^4 + Br^2 + C}\,dr\,d\theta \\ &= \frac{1}{2\pi^2}\frac{1}{|\mathbf{x}|}\int_0^\infty \sin(r|\mathbf{x}|)\frac{Ar^3}{r^4 + Br^2 + C}\,dr. \end{aligned} \tag{2.9}$$

Using Residue Theory [12], we get

$$K^I_{WT}(|\mathbf{x}|) = \frac{A}{4\pi}\frac{1}{|\mathbf{x}|}e^{-|\mathbf{x}|\sqrt{|B|}/2}\left(\cos\left(\sqrt{3}\sqrt{|B|}|\mathbf{x}|/2\right)+\frac{\sqrt{3}}{3}\sin\left(\sqrt{3}\sqrt{|B|}|\mathbf{x}|/2\right)\right). \quad (2.10)$$

Therefore,

$$\widehat{K^{II}_{WT}}(\eta) = \widehat{K_{WT}}(\eta) - \widehat{K^I_{WT}}(\eta) = \mathcal{O}(\eta^{-6}), \quad |\eta| \gg 1, \quad (2.11)$$

so $K^{II}_{WT} \in C^2(\mathbb{R}^3)$, and $K^{II}_{WT}$ is uniformly bounded. Moreover, it can be shown that

$$K^{II}_{WT}(\mathbf{x}) \sim -\frac{1}{\pi}\frac{\cos(|\mathbf{x}|)}{|\mathbf{x}|^3}, \quad |\mathbf{x}| \gg 1. \quad (2.12)$$

A derivation of (2.12) is presented in Appendix A. The functions $K^I_{WT}$ and $K^{II}_{WT}$ are plotted in Figs. 4(a) and 4(b), respectively.

## 2.3 Pseudopotential

We have used the Goodwin-Needs-Heine (GNH) pseudopotential [13] in order to describe the electron-ion interactions in (1.10). The pseudopotential is given in Fourier space for a single atom as a radial function, and therefore it can be written in real space as

$$V_a(|\mathbf{x}|) = \frac{2}{\pi}\int_0^\infty \frac{\sin(|\mathbf{x}|r)}{|\mathbf{x}|r}\left((Z-AR)\cos(Rr)+A\frac{\sin(Rr)}{r}\right)e^{-(r/R_c)^6}\,dr, \quad (2.13)$$

where $Z$ is the valence, and the parameters $R_c$, $A$, and $R$ are given in [13]. For Aluminium, $Z = 3$, $R_c = 3.5$, $R = 1.150$, and $A = 0.1107$. Since $f(z) = \sin(z)/z$ is an entire function, it follows from (2.13) that $V_a$ is smooth, i.e., $V_a \in C^\infty([0,\infty))$.

The integral in (2.13) can be evaluated to machine precision using adaptive Gaussian quadrature [14], and it is plotted in Fig. 5. An electron located near the core of the atom will feel mostly the repulsion of the core electrons, whereas at far distances, the electron will feel the attraction of the nucleus, as its charge is unbalanced. As a consequence, the pseudopotential is repulsive at short distances, and attractive at long distances.

Once the pseudopotential for a single atom is computed, the pseudopotential for a system with $N_a$ atoms located at $\{R_i\}_{i=1}^{N_a}$ can be evaluated as

$$v(\mathbf{x}) = \sum_{i=1}^{N_a} V_a(|\mathbf{x}-\mathbf{R}_i|). \quad (2.14)$$

In our implementation only the pseudo-potential for one atom needs to be computed using (2.13). Then (2.14) is evaluated using cubic interpolation.

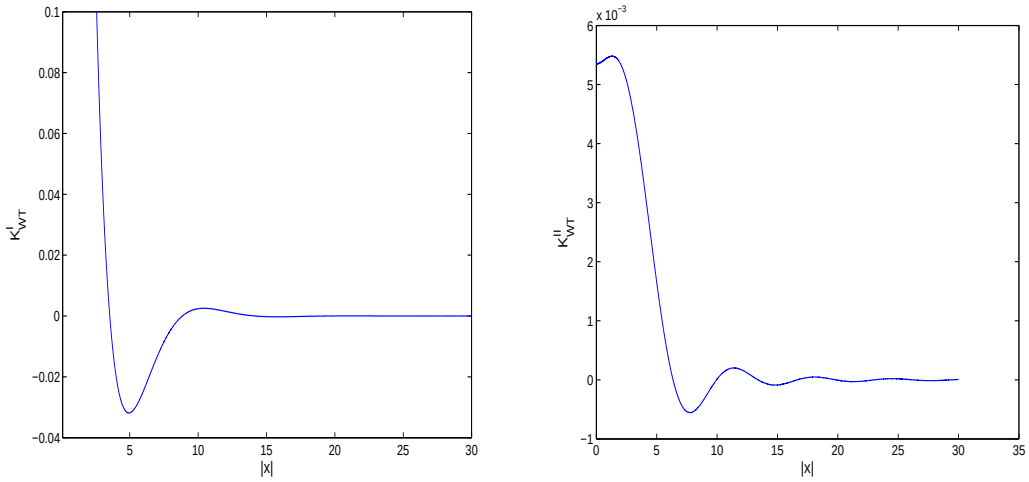


(a) (b)

Figure 4: (a) Singular term in the Wang-Teter kernel ($K^I_{WT}$). (b) Regular term in the decomposition of the Wang-Teter kernel ($K^{II}_{WT}$).

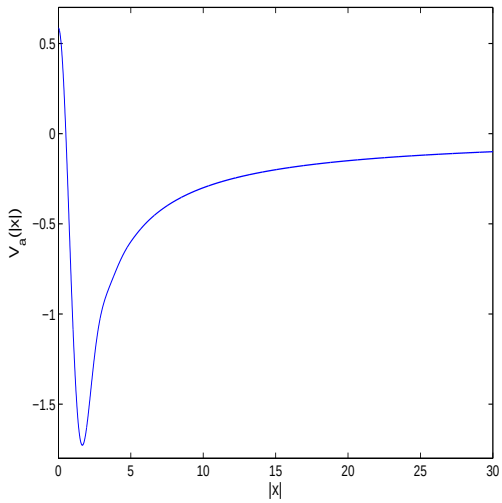


Figure 5: Goodwin-Needs-Heine pseudopotential for Aluminium. The potential is repulsive at short distances, and attractive at long distances.

## 2.4 Existence of minimizers and basic properties

The first theorem establishes the existence of minimizers of functional (1.10):

**Theorem 2.1** (Existence of minimizers)**.** *Given* $v \in C^\infty(\Omega)$ *and* $K_{WT}, K_H \in L^1_{loc}(\mathbb{R}^3)$. *Consider the problem*

$$\inf_{u\in\mathcal{B}} F[u], \tag{2.15}$$

*where $F$ and $\mathcal{B}$ are given in* (1.10) *and* (1.11)*, respectively. Then $\exists u^* \in \mathcal{B}$ such that*

$$F[u^*] = \min_{u\in\mathcal{B}} F[u]. \tag{2.16}$$

*Proof.* The proof follows from standard arguments in the Calculus of Variations [15], involving the Sobolev Embedding, and the Rellich-Kondrachov compactness theorem. □

In the following lemma we show that the minimum energy obtained in Theorem 2.1 coincides with the minimum energy of (1.10) when the non-negativity constraint is removed.

**Lemma 2.1.** *Under the same assumptions as Theorem* 2.1*, consider*

$$\mathcal{C} = \left\{ u \in H_0^1(V) \middle| \int_V u^2 = 1 \right\}, \tag{2.17}$$

*and the problem*

$$\inf_{u\in\mathcal{C}} F[u]. \tag{2.18}$$

*Then $\exists w^* \in \mathcal{C}$ such that*

$$F[w^*] = \min_{u\in\mathcal{C}} F[u], \tag{2.19}$$

*and moreover,*

$$F[|w^*|] = \min_{u\in\mathcal{B}} F[u]. \tag{2.20}$$

*Proof.* The existence of minimizers for the unconstrained problem follows similarly to the constrained case. Since $F[w^*] = F[|w^*|]$, it follows that the minimum energy obtained by functions in $\mathcal{B}$ coincides with the global, unconstrained minimum (2.19):

$$F[w^*] \leq F[u^*] \leq F[|w^*|] = F[w^*]. \tag{2.21}$$

This completes the proof of this lemma. □

The significance of Lemma 2.1 is that, since the constrained, nonnegative, minimizer of (1.10), $u^*$, has the same energy as the global, unconstrained, minimizer of (1.10), $w^*$, then $u^*$ must satisfy the same Euler-Lagrange equation as $w^*$. Therefore, the constraint $u \geq 0$ does not affect the Euler-Lagrange equation in this case. We summarize this in the following:

**Theorem 2.2** (Euler-Lagrange equation)**.** *Let $u^*$ be the nonnegative global minimizer of* (1.10) *obtained in Theorem* 2.1*. Then $u^*$ satisfies the elliptic equation*

$$\begin{aligned} -\Delta u - \frac{14C_{TF}N^{2/3}}{15}u^{7/3} + \frac{8C_{TF}N^{2/3}}{3}u^{2/3}K_{WT} * u^{5/3} + 2NuK_H * u^2 \\ - 2\left(\frac{3N}{\pi}\right)u^{5/3} + 2u\epsilon(Nu^2) + 2Nu^3\epsilon'(Nu^2) + 2v(\mathbf{x})u = \lambda u, \quad \mathbf{x}\in\Omega, \end{aligned} \tag{2.22}$$

*with boundary condition*

$$u = 0, \quad \mathbf{x} \in \partial\Omega. \tag{2.23}$$

*Proof.* Since $u^*$ is a global minimizer for the unconstrained problem, it follows that, for any $\phi \in H_0^1(\Omega)$, the function

$$g(t) = F\left[\frac{u^* + t\phi}{\|u^* + t\phi\|_2}\right], \quad t \in \mathbb{R}, \tag{2.24}$$

has a minimum at $t = 0$, and therefore $g'(0) = 0$. Since $\phi$ is arbitrary, equation (2.22) follows. □

The following theorem follows from regularity theory for solutions of second order elliptic equations [16]:

**Theorem 2.3** (Regularity)**.** *The minimizer $u^* \in C^{2,\alpha}(\overline{\Omega})$ for $\alpha \leq 1/2$. Furthermore, if $u(\mathbf{x}_0) = 0$ for some $\mathbf{x}_0 \in \Omega$, then $Du(\mathbf{x}_0) = 0$ and $D^2(\mathbf{x}_0) = 0$.*

Since the function $\epsilon(\rho)$ is only of class $C^1(\mathbb{R})$, we do not expect the solution to be more than $C^{2,\alpha}$ for $\alpha \leq 1/2$.

# 3 Numerical method

Consider the domain $\Omega = [0, L] \times [0, D] \times [0, H]$. We discretize $\Omega$ using a uniform mesh with grid sizes $\Delta x = L/n_x$, $\Delta y = D/n_y$, and $\Delta z = H/n_z$. We define the values of the density at the center of the cells: $u_{i,j,k} \approx u(x_i, y_j, z_k)$, where

$$\begin{aligned} x_i &= (i - 1/2)\ \Delta x, \quad i = 0, \dots, n_x + 1, \\ y_j &= (j - 1/2)\ \Delta y, \quad j = 0, \dots, n_y + 1, \\ z_k &= (k - 1/2)\ \Delta z, \quad k = 0, \dots, n_z + 1. \end{aligned} \tag{3.1}$$

The points with indices 0 or $n_x + 1$, $n_y + 1$, and $n_z + 1$ are ghost cells outside the computational domain, and are used only to impose the boundary conditions. Since the density is zero on the boundary, we define the ghost values by reflection, which on the $x = 0$ boundary would be: $u_{0jk} = -u_{1jk}$. A similar expression is used on the other boundaries.

Given two functions $f$ and $g$ defined on the grid, we define their inner product as $(f, g)_h = \Delta V \sum_{i,j,k} f_{ijk} g_{ijk}$, and the norm of $f$ as $\|f\| = (f, f)_h^{1/2}$. We define $|f|^p$ the function defined on the grid by $(|f|^p)_{ijk} = |f_{ijk}|^p$.

To approximate the convolution with the Hartree potential we approximate $u$ by a piecewise constant function:

$$K_H * u(x_i, y_j, z_k) \approx \sum_{r=1}^{n_x} \sum_{s=1}^{n_y} \sum_{p=1}^{n_z} u_{rsp} \int_{\Omega_{rsp}} \frac{1}{|\mathbf{x}_{ijk} - \mathbf{y}|}\, d\mathbf{y}, \tag{3.2}$$

where $\Omega_{rps} = [x_r - \Delta x/2, x_r + \Delta x/2] \times [y_s - \Delta y/2, y_s + \Delta y/2] \times [z_p - \Delta z/2, z_p + \Delta z/2]$, and $\mathbf{x}_{ijk} = (x_i, y_j, z_k)$. The integrals in (3.2) can be evaluated using a combination of explicit integration and adaptive Gaussian quadrature [14], and depend only on the distance

between $\mathbf{x}_{ijk}$ and $\mathbf{x}_{rsp}$. Defining

$$K_{i-r,j-s,k-p} = \int_{\Omega_{rsp}} \frac{1}{|\mathbf{x}_{ijk} - \mathbf{y}|}\, d\mathbf{y}, \tag{3.3}$$

we can write (3.2) as a discrete convolution:

$$(K * u)_{ijk} = \sum_{r=1}^{n_x} \sum_{s=1}^{n_y} \sum_{p=1}^{n_z} u_{rsp} K_{i-r,j-s,k-p}. \tag{3.4}$$

We can treat the convolution with the Wang-Teter kernel in a similar way. We can write the Wang-Teter kernel as

$$K_{WT}(\mathbf{x}) = \frac{A}{4\pi}\frac{1}{|\mathbf{x}|} + K_{smooth}(\mathbf{x}), \tag{3.5}$$

where

$$K_{smooth}(\mathbf{x}) = \left( K^I_{WT}(\mathbf{x}) - \frac{A}{4\pi}\frac{1}{|\mathbf{x}|} \right) + K^{II}_{WT}(\mathbf{x}). \tag{3.6}$$

The singular term in (3.5) is a multiple of the Hartree term discussed above. The other term in (3.5) is smooth, and the convolution with this term can be approximated by simply using the midpoint rule. We evaluate the discrete convolution (3.4) using the Fast Fourier Transform (FFT) with zero padding (see Appendix B).

We approximate the derivatives using forward differences:

$$\begin{aligned} \delta_x u_{ijk} &= \frac{u_{i+1,j,k} - u_{i,j,k}}{\Delta x}, \\ \delta_y u_{ijk} &= \frac{u_{i,j+1,k} - u_{i,j,k}}{\Delta y}, \\ \delta_z u_{ijk} &= \frac{u_{i,j,k+1} - u_{i,j,k}}{\Delta z}. \end{aligned} \tag{3.7}$$

The gradient term in the energy is approximated using the trapezoidal rule, which in the one-dimensional case would be:

$$\int |f'|^2\, dx = \Delta x \left( \frac{1}{2}|\delta_x f_0|^2 + \sum_{i=1}^{n_x - 1} |\delta_x f_i|^2 + \frac{1}{2}|\delta_x f_{n_x}|^2 \right) + \mathcal{O}(\Delta x^2). \tag{3.8}$$

We represent the summation on the right hand side of (3.8) by $\sum_i{}'$. The other terms in

the energy (1.10) are discretized using the midpoint rule:

$$\begin{aligned} F_h[u] &= \Delta V\Bigg(\frac{1}{2}{\sum_i}' \sum_{j=1}^{n_y}\sum_{k=1}^{n_z}\left|\frac{u_{i+1,j,k}-u_{i,j,k}}{\Delta x}\right|^2 + \frac{1}{2}\sum_{i=1}^{n_x}{\sum_j}'\sum_{k=1}^{n_z}\left|\frac{u_{i,j+1,k}-u_{i,j,k}}{\Delta y}\right|^2 \\ &+\frac{1}{2}\sum_{i=1}^{n_x}\sum_{j=1}^{n_y}{\sum_k}'\left|\frac{u_{i,j,k+1}-u_{i,j,k}}{\Delta z}\right|^2 + \sum_{i=1}^{n_x}\sum_{j=1}^{n_y}\sum_{k=1}^{n_z}\Bigg[-\frac{7C_{TF}N^{2/3}}{25}(u_{ijk})^{10/3} \\ &+\frac{4C_{TF}N^{2/3}}{5}(u_{ijk})^{5/3}(K_{WT}*u^{5/3})_{ijk} + \frac{N}{2}(u_{ijk})^2\,(K_H*u^2)_{ijk} \\ &-\frac{3}{4}\left(\frac{3N}{\pi}\right)^{1/3}(u_{ijk})^{8/3} + (u_{ijk})^2\varepsilon(N(u_{ijk})^2) + v_{ijk}(u_{ijk})^2\Bigg]\Bigg). \end{aligned} \tag{3.9}$$

### 3.1 Algorithm for energy minimization

Newton-based methods have been very successful in large-scale unconstrained minimization problems [17, 18]. We present here a modification of the Truncated-Newton method appropriate for constrained minimization, under the constraints $\|u\|_h = 1$, and $u \geq 0$.

Most algorithms for energy minimization consist of two iterations: An inner iteration, in which a direction along which the energy decreases (i.e. a *descent direction*) is constructed, and an outer iteration, in which energy is approximately minimized along the descent direction. In Newton-based minimization methods, given an approximation $u^{(k)}$, the energy is approximated around $u^{(k)}$ by a quadratic functional, which is subsequently minimized to produce a descent direction, $p$. The new approximation is $u^{(k+1)} = u^{(k)} + \alpha p$, where $\alpha$ is usually chosen performing a line search.

In Theorem 2.2 we showed that the criticality condition is not affected by the constraint $u \geq 0$. As a consequence, we can deal with the two constraints separately: The non-negativity constraint is imposed in the line search alone. The unit norm constraint plays an intergral role in the construction of the local approximation, and in the line search as well.

We approximate the energy, locally, by a quadratic functional:

$$F\left[\frac{u+p}{\|u+p\|}\right] = F[u] + (G[u],p)_h + \frac{1}{2}(H[u]\cdot p, p)_h + \mathcal{O}(|p|^3). \tag{3.10}$$

In minimization without constraints, $G$ and $H$ are the gradient and Hessian of the energy, respectively. In the constrained problem (1.10)-(1.11), $G$ and $H$ are projected versions of the gradient and Hessian, respectively. The projected gradient is

$$G[u] = \Pi_u\left(\nabla F[u]\right) = \nabla F[u] - (\nabla F[u], u)_h\, u, \tag{3.11}$$

where $\nabla F[u]$ is the unconstrained gradient, obtained from the discrete energy taking partial derivatives with respect to the variables $\{u_{ijk}\}$. In (3.11) $\Pi_u$ denotes the projection operator defined by $\Pi_u(v) = v - (u,v)_h u$.y.

In practice, often we do not need to compute the Hessian explicitly, but rather the action of the Hessian on a vector, which can be obtained from (3.10):

$$H[u]\cdot p=\Pi_u\left(\nabla^2F[u]\cdot\Pi_u(p)\right)-(\nabla F[u],p)_h u-(\nabla F[u],u)_h p-(u,p)_h\nabla F[u], \quad (3.12)$$

The Hessian matrix $\nabla^2 F[u]$ is the matrix containing the second derivatives of the energy with respect to $u_{ijk}$.

The Euler-Lagrange equation is $G[u]=0$, or

$$\nabla F[u]=(\nabla F[u],u)_h u. \quad (3.13)$$

Note that equation (3.13) is a nonlinear eigenvalue problem, equivalent to

$$\nabla F[u]=\lambda u. \quad (3.14)$$

We consider here equation (3.13) as a nonlinear equation, rather than an equation with a Lagrange multiplier.

When we minimize the quadratic part of (3.10), we obtain that $p$ satisfies the linear equation

$$H[u]\cdot p=-G[u]. \quad (3.15)$$

The matrix $H[u]$ is symmetric, but not necessarily positive definite. We use the Preconditioned Conjugate Gradient (PCG) to solve equation (3.15). For the preconditioner we use the Laplacian term, which in our discretization can be inverted using the FFT. If $H[u]$ is not positive definite, the procedure fails by producing a direction of negative curvature. In that case we use the corresponding approximation to the solution of system (3.15) as our descent direction. Sufficiently near the minimum, $H[u]$ becomes positive definite, and from (3.15) we get $p=-H[u]^{-1}\cdot G[u]$, i.e., Newton's method. For details regarding the convergence of this algorithm in the unconstrained case, see [18].

Given an approximation to the minimizer of (3.9), $u^{(k)}$, and a descent direction, $p$, the next approximation is computed with a line search using

$$f(\epsilon)=F\left[\frac{|u^{(k)}+\epsilon p|}{\|u^{(k)}+\epsilon p\|}\right]. \quad (3.16)$$

In our line search we impose the Wolf conditions to ensure sufficient decrease in the energy [18].

# 4 Numerical examples

We illustrate the efficiency and convergence properties of the method with several examples. In the first example, we compute the first eigenvalue and corresponding eigenfunction of the Laplacian in a rectangular box by minimizing

$$F[u]=\frac{1}{2}\int|\nabla u|^2. \quad (4.1)$$

Table 1: Errors in the computation of the first eigenvalue of the Laplacian in the box $[0,1]\times[0,2]\times[0,4]$. Also included is the number of iterations in the outer loop (line search) and the inner loop (PCG).

| h | # Line searches | # PCG steps | $e(h)=\lvert\lambda-\lambda(h)\rvert$ | $\log(e(h)/e(h/2))/\log(2)$ |
|---|---|---|---|---|
| 1/8 | 7 | 25 | $6.72984\times10^{-2}$ | |
| 1/16 | 6 | 27 | $1.68865\times10^{-2}$ | 1.99470 |
| 1/32 | 8 | 33 | $4.22550\times10^{-3}$ | 1.99868 |
| 1/64 | 7 | 16 | $1.05662\times10^{-3}$ | 1.99967 |
| 1/128 | 8 | 25 | $2.64170\times10^{-4}$ | 1.99992 |

Table 2: Minimum energy for one single Aluminium atom in an empty cubic box of dimension 5Å. In dimensionless variables the length is $L=5/a_0=9.44863$, where $a_0$ is the Bohr radius. The Thomas-Fermi-von Weizsacker energy with the correction of Wang and Teter was used.

| h | Minimum | $e(h)=\lvert E(h)-E_\infty\rvert$ | $\log(e(h)/e(h/2))/\log(2)$ |
|---|---|---|---|
| L/16 | -0.77218 | $7.83991\times10^{-3}$ | |
| L/32 | -0.76622 | $1.87643\times10^{-3}$ | 2.06285 |
| L/64 | -0.76479 | $4.43479\times10^{-4}$ | 2.08105 |
| L/128 | -0.76443 | $8.86834\times10^{-5}$ | 2.32213 |
| L/256 | -0.76434 | 0 | |

The domain has dimensions $L\times D\times W$. The eigenfunction is

$$u(x,y,z)=\frac{8}{LDW}\sin\left(\frac{\pi x}{L}\right)\sin\left(\frac{\pi y}{D}\right)\sin\left(\frac{\pi z}{W}\right), \tag{4.2}$$

which is also an eigenvector of the discrete Laplacian when restricted to the grid. The corresponding eigenvalue is $\lambda=\pi^2\left(\frac{1}{L^2}+\frac{1}{D^2}+\frac{1}{W^2}\right)$, and the minimum energy is $\lambda/2$. The results of the minimization are presented in Table 1. The errors in the eigenvalue indicate that second order accuracy is achieved: $e(h)=\mathcal{O}(h^2)$. The number of line searches needed corresponds to the number of iterations in Newton's method (outer loop). The number of PCG steps is a measure of the total number of operations. The number of iterations in both loops is stable, almost independent of the number of grid points.

In our second example we consider a single Aluminium atom enclosed in an empty box of side 5Å. In atomic units, the size of the box is $L=5/a_0=9.44863062496795$, where $a_0=5.291772108\times10^{-11}$ is the Bohr radius. We minimize the Thomas-Fermi-von Weizsacker energy with the corrections of Wang and Teter (1.10). The results are shown in Table 2. The energy obtained using $256^3$ grid points is taken to be the exact value.

In our third example, we consider an Aluminium sample in an FCC lattice, with three unit cells in each direction, totaling 172 atoms, and estimate the optimal lattice constant, $a$, for the FCC configuration. We do this by minimizing energy (1.10) for a range of values of the lattice constant. We used $128^3$ mesh points. When the interactions between the

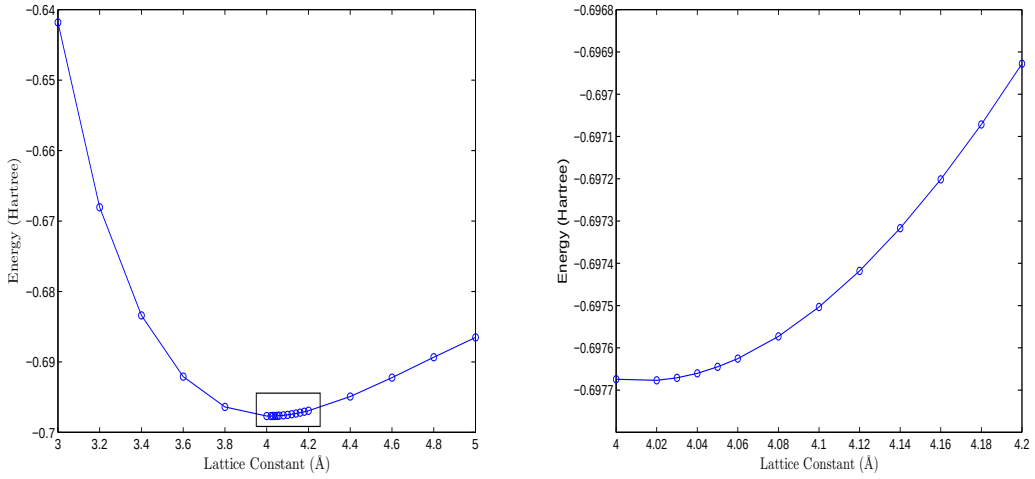


(a) (b)

Figure 6: (a) Energy as a function of the lattice constant for Aluminium FCC. A refinement was used in the interval $[4, 4.2]$. (b) The refined region enclosed in the rectangle.

nuclei are taken into account, the total energy becomes

$$E_T[u] = E[u] + \frac{Z^2}{N} \sum_{i<j} \frac{1}{|\mathbf{R}_i - \mathbf{R}_j|}, \tag{4.3}$$

where $E[u]$ is given in (1.10), and $\mathbf{R}_i$, $i = 1, 2, \cdots, M$, are the locations of the nuclei. This inter-ionic energy does not depend on the density $u$ and therefore only needs to be computed once, and does not enter the Euler-Lagrange equations. Since the experimentally obtained value is 4.05Å, we refined our search in the interval $[4, 4.2]$. We plot the energy as a function of the lattice constant in Fig. 6(a). In Fig. 6(b) we show the refinement enclosed in the rectangle in Fig. 6(a). The optimal lattice parameter for energy (1.10) was found to be 4.02Å, with $E = -0.697677$ Hartree per electron.

In our final example, we consider 365 Aluminium atoms in an FCC lattice. In Table 3 we show the results of the minimization for various resolutions. The energy obtained with $256^3$ grid points is taken to be the correct value. We stop the minimization when $\|G[u]\| \leq 10^{-8}$. The progress in a typical run is shown in Table 4, illustrating the convergence of our method, characteristic of Newton-based iterations. The three-dimensional electronic structure is shown in Fig. 7, where we show an iso-surface plot of the electron density. Finally, an interior slice in the $YZ$-plane is shown in Fig. 8. The electron density is highest in an annulus around the ions, consistent with the shape of the pseudopotential (see Fig. 5).

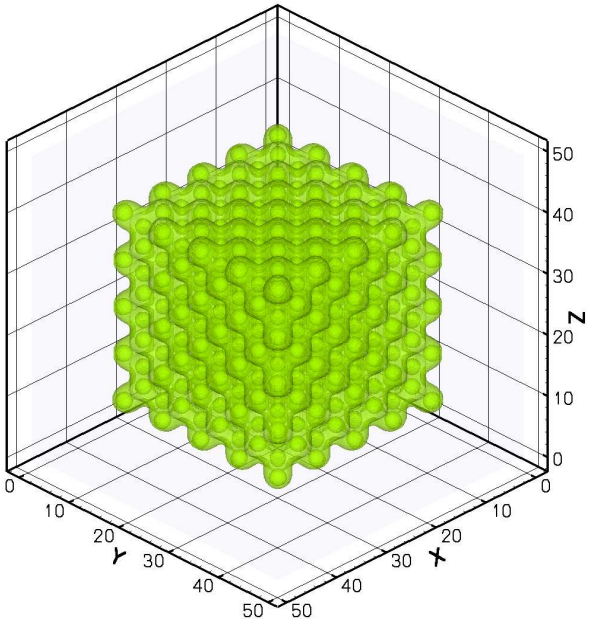


Figure 7: Iso-surface plot of the electron density in the Aluminium FCC lattice with $365$ atoms. The electron density is normalized so that $\int \rho = 1$.

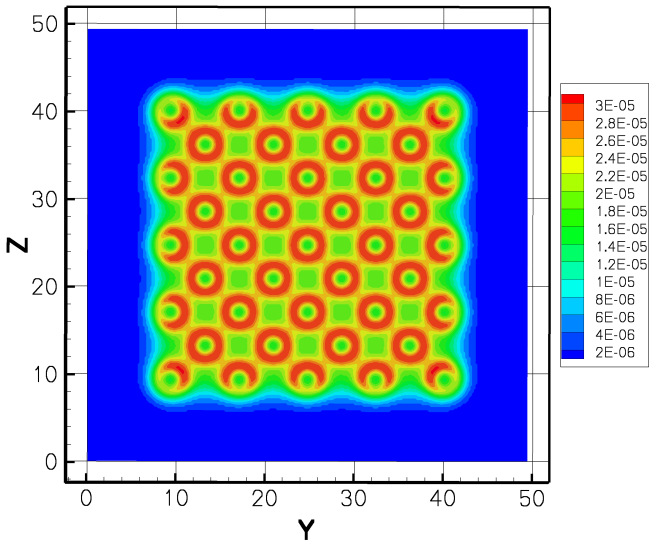


Figure 8: Contour plot of the electron density in an interior slice in the $YZ$-plane. The density concentrates in an annulus around the nuclei.

Table 3: Energy minimization for 365 Aluminium atoms in an FCC lattice. The Thomas-Fermi-von Weizsacker energy with the correction of Wang and Teter was used.

| h | Minimum | $e(h) = \|E(h) - E_\infty\|$ | $\log(e(h)/e(h/2))/\log(2)$ |
|---|---|---|---|
| 20/16 | -30.18562 | $2.76107 \times 10^{-1}$ | |
| 20/32 | -29.95795 | $4.84362 \times 10^{-2}$ | 2.51107 |
| 20/64 | -29.91566 | $6.14045 \times 10^{-3}$ | 2.97967 |
| 20/128 | -29.91055 | $1.03638 \times 10^{-3}$ | 2.56680 |
| 20/256 | -29.90952 | 0 | |

Table 4: Size of the (projected) gradient of the energy in a typical run. This is a measure of how closely the Euler-Lagrange equations are satisfied.

| $k$ | 1 | 2 | 3 | 4 | 5 | 6 | 7 | 8 | 9 | 10 |
|---|---|---|---|---|---|---|---|---|---|---|
| $\|G[u^{(k)}]\|$ | 146.68 | 13.57 | 6.47 | 4.93 | 0.62 | 5.24E-2 | 1.73E-2 | 1.54E-3 | 1.52E-5 | 1.36E-9 |

# 5 Conclusions

In conclusion, we have presented a second order accurate, efficient implementation of the Truncated Newton method for Orbital-Free Density-Functional Theory. The behavior of the Wang-Teter kernel at near and far distances has been determined. It was proved that the constrained problem (1.10)-(1.11) has nonnegative minimizers, and that they satisfy the same elliptic partial differential equation as the minimizers with no sign restriction. This allows us to deal with the two constraints in (1.11) separately: The unit length constraint is imposed both in the line search, and in the Newton step, where the projected gradient and Hessian are used. The non-negativity constraint in imposed in the line search procedure by taking absolute values. The efficiency of the method has been illustrated by computing the minimum energy of an Aluminum FCC lattice.

# A Decay of the Wang-Teter kernel

The Wang-Teter can be written in Fourier space as

$$\widehat{K_{WT}}(\eta) = \frac{2}{1 + \frac{1-|\eta|^2}{2|\eta|}\log\left|\frac{1-|\eta|}{1+|\eta|}\right|} - 3|\eta|^2 + \frac{3}{5}. \tag{A.1}$$

Since the Fourier transform only depends on $|\eta|$, the kernel will only depend on $|\mathbf{x}|$ in real space, and

$$K_{WT}(\mathbf{x}) = \frac{1}{2\pi^2|\mathbf{x}|}\int_0^\infty r\widehat{K_{WT}}(r)\sin(r|\mathbf{x}|)\,dr = \frac{1}{2\pi^2|\mathbf{x}|}\Im\int_0^\infty r\widehat{K_{WT}}(r)e^{i|\mathbf{x}|r}\,dr. \tag{A.2}$$

Note that a change to spherical coordinates was performed to obtain (A.2).

To obtain the behavior of (A.2) for $|\mathbf{x}| \gg 1$ we use path integration in the complex plane. Since the integrand has logarithmic terms, we split the integral between $[0,1]$ and $[1,\infty)$. We use the paths described in Fig. 9. We define $\Gamma_1 = \Gamma_{11} \cup \Gamma_{12} \cup \Gamma_{13} \cup \Gamma_{14}$ and $\Gamma_2 = \Gamma_{21} \cup \Gamma_{22} \cup \Gamma_{23} \cup \Gamma_{24} \cup \Gamma_{25}$.

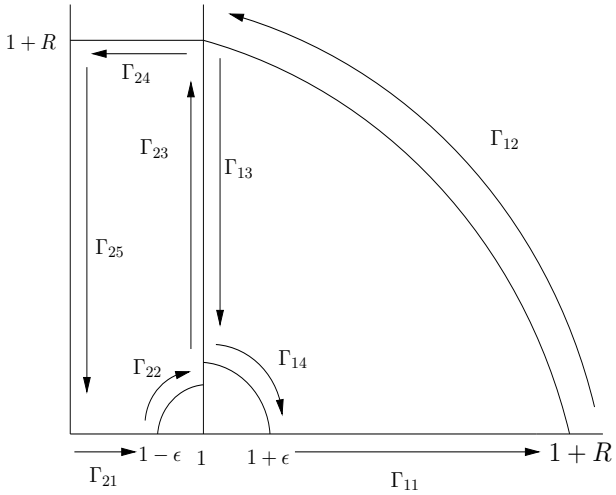


Figure 9: Paths used in the integration.

We consider first the region inside $\Gamma_1$. In that region, define

$$f(z) = \frac{2}{1 + \frac{1-z^2}{2z} \log\left(\frac{z-1}{z+1}\right)} - 3z^2 + \frac{3}{5}. \tag{A.3}$$

Note that any pole of $f$ inside $\Gamma_1$ will produce a residual term that decays exponentially fast as $|\mathbf{x}| \to \infty$, which will not affect the leading term in the expansion. In what follows we will assume that the Wang-Teter kernel has no poles inside $\Gamma_1$ or $\Gamma_2$, and understand equalities to be satisfied up to exponentially small terms in $|\mathbf{x}|$. With this in mind, we get

$$0 = \int_{\Gamma_1} e^{i|\mathbf{x}|z} z f(z)\, dz = \sum_{i=1}^{4} \int_{\Gamma_{1i}} z e^{i|\mathbf{x}|z} f(z)\, dz. \tag{A.4}$$

Now,

$$\lim_{\epsilon\to 0, R\to\infty} \int_{\Gamma_{11}} z e^{i|\mathbf{x}|z} f(z)\, dz = \int_1^\infty r e^{i|\mathbf{x}|r} \widehat{K_{WT}}(r)\, dr, \tag{A.5}$$

$$\lim_{R\to\infty} \int_{\Gamma_{12}} z e^{i|\mathbf{x}|z} f(z)\, dz = 0, \tag{A.6}$$

$$\lim_{\epsilon\to 0, R\to\infty} \int_{\Gamma_{13}} z e^{i|\mathbf{x}|z} f(z)\, dz = -i \int_0^\infty (1+ir) e^{i|\mathbf{x}|(1+ir)} f(1+ir)\, dr, \tag{A.7}$$

and

$$\lim_{\epsilon\to 0}\int_{\Gamma_{14}} ze^{i|\mathbf{x}|z}f(z)\,dz = 0. \tag{A.8}$$

Therefore, to leading order,

$$\int_1^\infty e^{i|\mathbf{x}|r}r\widehat{K_{WT}}(r)\,dr = ie^{i|\mathbf{x}|}\int_0^\infty (1+ir)e^{-|\mathbf{x}|r}f(1+ir)\,dr. \tag{A.9}$$

Now we consider the region inside $\Gamma_2$. In this region, we define

$$g(z) = \frac{2}{1+\frac{1-z^2}{2z}\log\left(\frac{1-z}{1+z}\right)} - 3z^2 + \frac{3}{5}. \tag{A.10}$$

In an similar way to how the integral on $\Gamma_1$ was treated, we get

$$0 = \int_{\Gamma_2} e^{i|\mathbf{x}|z}zg(z)\,dz = \sum_{i=1}^5 \int_{\Gamma_{2i}} ze^{i|\mathbf{x}|z}g(z)\,dz. \tag{A.11}$$

Now,

$$\lim_{\epsilon\to 0}\int_{\Gamma_{21}} ze^{i|\mathbf{x}|z}g(z)\,dz = \int_0^1 re^{i|\mathbf{x}|r}\widehat{K_{WT}}(r)\,dr, \tag{A.12}$$

$$\lim_{\epsilon\to 0}\int_{\Gamma_{22}} ze^{i|\mathbf{x}|z}g(z)\,dz = 0, \tag{A.13}$$

$$\lim_{\epsilon\to 0,R\to\infty}\int_{\Gamma_{23}} ze^{i|\mathbf{x}|z}g(z)\,dz = i\int_0^\infty (1+ir)e^{i|\mathbf{x}|(1+ir)}g(1+ir)\,dr, \tag{A.14}$$

$$\lim_{R\to\infty}\int_{\Gamma_{24}} ze^{i|\mathbf{x}|z}g(z)\,dz = 0, \tag{A.15}$$

and

$$\lim_{\epsilon\to 0}\int_{\Gamma_{25}} ze^{i|\mathbf{x}|z}g(z)\,dz = -i\int_0^\infty (ir)g(ir)e^{-|\mathbf{x}|r}\,dr. \tag{A.16}$$

Therefore, to leading order,

$$\int_0^1 e^{i|\mathbf{x}|r}r\widehat{K_{WT}}(r)\,dr = -ie^{i|\mathbf{x}|}\int_0^\infty (1+ir)e^{-|\mathbf{x}|r}g(1+ir)\,dr - \int_0^\infty rg(ir)e^{-|\mathbf{x}|r}\,dr. \tag{A.17}$$

As a consequence of Watson's lemma [19], the asymptotic behavior of the last term is

$$\begin{aligned}\Im\int_0^\infty rg(ir)e^{-|\mathbf{x}|r}\,dr &\sim \Im\int_0^\infty r(g(0)+ig'(0)r)e^{-|\mathbf{x}|r}\,dr \\ &\sim g'(0)\int_0^\infty r^2e^{-|\mathbf{x}|r}\,dr = \mathcal{O}\left(\frac{1}{|\mathbf{x}|^3}\right).\end{aligned} \tag{A.18}$$

Therefore we have

$$K_{WT}(|\mathbf{x}|) = \frac{1}{2\pi^2|\mathbf{x}|}\Im\left[ie^{i|\mathbf{x}|}\int_0^\infty (1+ir)e^{-|\mathbf{x}|r}\left(f(1+ir)-g(1+ir)\right)\,dr\right] + \mathcal{O}\left(\frac{1}{|\mathbf{x}|^4}\right). \tag{A.19}$$

Now,

$$\begin{aligned} & f(1+ir)-g(1+ir) \\ = & \frac{2}{1-i\frac{(2+ir)r}{2(1+ir)}\log\left(\frac{ir}{2+ir}\right)} - \frac{2}{1-i\frac{(2+ir)r}{2(1+ir)}\log\left(\frac{-ir}{2+ir}\right)} \\ = & 2\sum_{k=0}^\infty \left(i\frac{(2+ir)r}{2(1+ir)}\right)^k \left[\left(\log\left(\frac{ir}{2+ir}\right)\right)^k - \left(\log\left(\frac{-ir}{2+ir}\right)\right)^k\right]. \end{aligned} \tag{A.20}$$

The term for $k=0$ cancels, and the leading term is $k=1$:

$$2i\frac{(2+ir)r}{2(1+ir)}i\pi = -\pi\frac{(2+ir)}{1+ir}r. \tag{A.21}$$

By Watson's lemma,

$$K_{WT}(\mathbf{x}) \sim \frac{1}{2\pi^2|\mathbf{x}|}\Im\left[ie^{i|\mathbf{x}|}\int_0^\infty (-2\pi)re^{-r|\mathbf{x}|}\,dr\right] = -\frac{1}{\pi}\frac{\cos(|\mathbf{x}|)}{|\mathbf{x}|^3}, \quad |\mathbf{x}| \gg 1. \tag{A.22}$$

# B Numerical convolutions using the FFT

Given the discrete functions $\{u_r\}_{r=0}^{M-1}$, $\{K_s\}_{s=-M+1}^{M-1}$, we want to evaluate the discrete convolution of $u$ and $K$, defined as

$$(u*K)_j = \sum_{r=0}^{M-1} u_r K_{j-r}, \qquad j=0,\dots,M-1. \tag{B.1}$$

A direct summation procedure for (B.1) requires $\mathcal{O}(M^2)$ operations, and becomes prohibitively expensive for relative small values of $M$. A reduction in the number of operations to $\mathcal{O}(M\log_2 M)$ can be achieved by evaluating (B.1) using the Fast Fourier Transform (FFT). Although the procedure is well known, we include it here for completeness, in an attempt to make this article self-contained. More details can be found in [20].

Given $\{u_r\}_{r=0}^{M-1}$, the Discrete Fourier Transform of $u$, represented by $\widehat{u} = FFT(u,M)$, is defined by

$$\widehat{u}_s = \sum_{r=0}^{M-1} u_r e^{-\frac{2\pi irs}{M}}, \qquad s=0,\dots,M-1. \tag{B.2}$$

The values of $u$ can be recovered with the Inverse Discrete Fourier Transform, denoted by $u = iFFT(\widehat{u},M)$:

$$u_r = \frac{1}{M}\sum_{s=0}^{M-1} \widehat{u}_s e^{\frac{2\pi irs}{M}}, \qquad r=0,\dots,M-1. \tag{B.3}$$

The procedure to evaluate (B.1) using the Fast Fourier Transform is based on the following theorem:

**Theorem B.1** (Discrete Convolution Theorem)**.** *Consider the discrete functions* $\{u_r\}_{r=0}^{M-1}$ *and* $\{K_r\}_{r=0}^{M-1}$*, and assume they are periodic of period* $M$*. Consider*

$$(u*K)_r = \sum_{j=0}^{M-1} u_j K_{r-j}. \tag{B.4}$$

*Then the Discrete Fourier Transform of* $u*K$ *satisfies*

$$\widehat{(u*K)}_s = \widehat{u}_s \widehat{K}_s, \quad s = 0, \dots, M-1. \tag{B.5}$$

*Proof.* Since the convolution kernel is periodic of period $M$,

$$\begin{aligned} u_j &= \frac{1}{M} \sum_{s=0}^{M-1} \widehat{u}_s e^{\frac{2\pi i j s}{M}}, \quad r = 0, \dots, M-1, \\ K_{r-j} &= \frac{1}{M} \sum_{s=0}^{M-1} \widehat{K}_s e^{\frac{2\pi i (r-j) s}{M}}, \quad r = 0, \dots, M-1. \end{aligned} \tag{B.6}$$

Therefore,

$$\begin{aligned} (u*K)_r &= \frac{1}{M^2} \sum_{s=0}^{M-1} \sum_{p=0}^{M-1} \widehat{u}_s \widehat{K}_p \sum_{j=0}^{M-1} e^{\frac{2\pi i j s}{M}} e^{\frac{2\pi i (r-j) p}{M}} \\ &= \frac{1}{M^2} \sum_{s=0}^{M-1} \sum_{p=0}^{M-1} \widehat{u}_s \widehat{K}_p e^{\frac{2\pi i r p}{M}} \sum_{j=0}^{M-1} e^{\frac{2\pi i (s-p) j}{M}} = \frac{1}{M} \sum_{p=0}^{M-1} \widehat{u}_p \widehat{K}_p e^{\frac{2\pi i r p}{M}}, \end{aligned} \tag{B.7}$$

where we have used the fact that

$$\sum_{j=0}^{M-1} e^{\frac{2\pi i (s-p) j}{M}} = \begin{cases} 0 & \text{if } s \neq p, \\ M & \text{otherwise.} \end{cases} \tag{B.8}$$

The theorem follows from (B.7) and (B.3). □

In the general case the discrete kernel is not periodic, and Theorem B.1 cannot be applied directly. However, this can be circumvented by padding $u$ with zeroes, at the expense of computing the FFT with twice as many points in each direction:

**Theorem B.2** (Non-Periodic Discrete Convolution Theorem)**.** *Consider the discrete functions* $\{u_r\}_{r=0}^{M-1}$ *and* $\{K_r\}_{r=0}^{M-1}$*. Define* $\widetilde{u}$ *and* $\widetilde{K}$ *by*

$$\widetilde{u}_r = \begin{cases} u_r & r = 0, \dots, M-1, \\ 0 & r = M, \dots, 2M-1. \end{cases} \tag{B.9}$$

$$\widetilde{K}_r = \begin{cases} K_r & r = 0, \dots, M-1, \\ 0 & r = M, \\ K_{r-2M} & r = M, \dots, 2M-1. \end{cases} \tag{B.10}$$

*We extend* $\widetilde{u}$ *and* $\widetilde{K}$ *periodically, with period* $2M$*, so that* $\widetilde{u}_{i+2M} = \widetilde{u}_i$*, and* $\widetilde{K}_{i+2M} = \widetilde{K}_i$*,* $\forall i \in \mathbb{Z}$*. Then,*

$$(u * K)_r = (\widetilde{u} * \widetilde{K})_r \quad r = 0, \dots, M-1. \tag{B.11}$$

*Define* $\widehat{u} = FFT(\widetilde{u}, 2M)$*,* $\widehat{K} = FFT(\widetilde{K}, 2M)$*, and* $\widehat{u * K} = FFT(u * K, 2M)$*. Then,*

$$(\widehat{u * K})_s = \widehat{u}_s \widehat{K}_s. \tag{B.12}$$

*Proof.* Since $\widetilde{u}_r = 0$ for $r = M, \dots, 2M-1$,

$$(\widetilde{u} * \widetilde{K})_r = \sum_{j=0}^{2M-1} \widetilde{u}_j \widetilde{K}_{r-j} = \sum_{j=0}^{M-1} u_j K_{r-j} = (u * K)_r, \quad r = 0, \dots, M-1. \tag{B.13}$$

The remaining of the proof is identical to the proof in Theorem B.1, since $\widetilde{u}$ and $\widetilde{K}$ are periodic. □

In Algorithm 1 below we describe the procedure for the fast evaluation of discrete convolutions using the FFT. Note that most popular implementations of the FFT are not normalized, i.e., an application of the forward transform followed immediately by an application the backward transform will multiply the array by a constant factor, dependent on the implementation, which is usually a multiple of the size of the array. As a consequence, an additional step must be performed in Algorithm 1 to normalize the output.

**Algorithm 1** Discrete Convolution using FFT - Non-periodic case

1: Given $u_i$, $i = 0, \dots, N-1$, and $K_r$, $r = -N+1, \dots, 0, \dots, N-1$.
2: Define

$$\widetilde{u}_i = \begin{cases} u_i & i = 0, \dots, N-1 \\ 0 & i = N, \dots, 2N-1 \end{cases} \tag{B.14}$$

and

$$\widetilde{K}_i = \begin{cases} K_i & i = 0, \dots, N-1 \\ 0 & i = N \\ K_{i-2N} & i = N+1, \dots, 2N-1 \end{cases} \tag{B.15}$$

3: Compute the FFTs: $\widehat{u} = FFT(\widetilde{u}, 2N)$, $\widehat{K} = FFT(\widetilde{K}, 2N)$.
4: Multiply in Fourier Space:

$$\widehat{v}_r = \widehat{u}_r \widehat{K}_r, \quad r = 0, \dots, 2N-1. \tag{B.16}$$

5: Compute the inverse FFT: $\widetilde{v} = iFFT(\widehat{v}, 2N)$.
6: Then $(u * K)_i = \widetilde{v}_i$, for $i = 0, \dots, N-1$.

## Acknowledgments

I would like to thank Prof. Weinan E for suggesting this problem to me. I would also like to thank Prof. Emily A. Carter, and the members of her group, in particular Gregory Ho and Vincent Ligneres, for explaining to me some of the intricacies of OFDFT. The simulations presented in this article were carried out in an HP workstation purchased with funds provided by NSF grant DMS-0411504; in a Beowulf cluster purchased by the Mathematics department at UCSB with funds provided by an NSF SCREMS grant DMS-0112388; and in an SGI Altix system located at the CNSI Computer Facilities at UCSB, purchased with funds provided by NSF grant CHE-0321368.

### References

[1] L. H. Thomas, The calculation of atomic fields, Proc. Camb. Phil. Soc., 23 (1927), 542-548.
[2] E. Fermi, Un metodo statistice per la determinazione di alcune propieta dell'atomo, Rend. Accad. Lincei, 6 (1927), 602-607.
[3] P. Hohenberg and W. Kohn, Inhomogeneous electron gas, Phys. Rev., 136(3B) (1964), 864-871.
[4] R. G. Parr and W. Yang, Density-Functional Theory of Atoms and Molecules, International Series of Monographs on Chemistry, Oxford University Press, New York, 1989.
[5] W. Kohn and L. J. Sham, Self-consistent equations including exchange and correlation effects, Phys. Rev., 140(4A) (1965), 1133-1138.
[6] C. F. von Weizsacker, Zur theorie dier kernmassen, Z. Physik, 96 (1935), 431-458.
[7] L. W. Wang and M. P. Teter, Kinetic-energy functional of the electron-density, Phys. Rev. B, 45(23) (1992), 13196-13220.
[8] Y. A. Wang, N. Govind and E. A. Carter, Orbital-free kinetic-energy density functionals with a density-dependent kernel, Phys. Rev. B, 60(24) (1999), 16350-16358.
[9] Y. A. Wang and E. A. Carter, Orbital-free kinetic-energy density functional theory, in: S. D. Schwartz (Ed.), Theoretical Methods in Condensed Phase Chemistry, Progress in Theoretical Chemistry and Physics, Kluwer, 2000, pp. 117-84.
[10] B. J. Zhou, V. L. Ligneres and E. A. Carter, Improving the orbital-free density functional theory description of covalent materials, J. Chem. Phys., 122(4) (2005), 4103.
[11] J. P. Perdew and A. Zunger, Self interaction correction to density functional approximations for many electron systems, Phys. Rev. B, 23(10) (1981), 5048-5079.
[12] L. V. Ahlfors, Complex Analysis, 3rd ed., McGraw-Hill, 1979.
[13] L. Goodwin, R. J. Needs and V. Heine, A pseudopotential total energy study of impurity-promoted intergranular embrittlement, J. Phys.-Condens. Mat., 2 (1990), 351-365.
[14] E. Isaacson and H. B. Keller, Analysis of Numerical Methods, John Wiley & Sons, Inc., New York, 1966.
[15] B. Dacorogna, Direct Methods in the Calculus of Variations, Applied Mathematical Sciences, 78, Springer-Verlag, Berlin-New York, 1989.
[16] D. Gilbarg and N. S. Trudinger, Elliptic Partial Differential Equations of Second Order, Classics in Mathematics, Springer-Verlag, Berlin, 2001. Reprint of the 1998 edition.
[17] R. S. Dembo and T. Steihaug, Truncated-Newton algorithms for large-scale unconstrained optimization, Math. Program., 26 (1983), 190-212.

[18] J. Nocedal and S. J. Wright, Numerical Optimization, Springer Series in Operations Research, Springer-Verlag, New York, 1999.
[19] N. Bleistein and R. A. Handelsman, Asymptotic Expansions of Integrals, Dover, New York, 1975.
[20] H. J. Nussbaumer, Fast Fourier Transform and Convolution Algorithms, Springer Series in Information Sciences, Volume 2, Springer-Verlag, Berlin, 1981.